International Journal of Heat and Mass Transfer 138 (2019) 738–749

Contents lists available at ScienceDirect

International Journal of Heat and Mass Transfer

journal homepage: www.elsevier.com/locate/ijhmt

Natural convective flow and heat transfer of Nano-Encapsulated Phase Change Materials (NEPCMs) in a cavity

Mohammad Ghalambaz [a,*], Ali J. Chamkha [b,c], Dongsheng Wen [a,d,*]

[a] School of Aeronautic Science and Engineering, Beihang University, Beijing, PR China
[b] Mechanical Engineering Department, Prince Mohammad Endowment for Nanoscience and Technology, Prince Mohammad Bin Fahd University, Al-Khobar 31952, Saudi Arabia
[c] RAK Research and Innovation Center, American University of Ras Al Khaimah, P.O. Box 10021, Ras Al Khaimah, United Arab Emirates
[d] School of Chemical and Process Engineering, University of Leeds, Leeds, UK

ARTICLE INFO

Article history:
Received 12 January 2019
Received in revised form 7 April 2019
Accepted 7 April 2019
Available online 28 April 2019

Keywords:
Nano Encapsulated Phase Change Materials (NEPCMs)
Free convection heat transfer
Heat transfer enhancement

ABSTRACT

Free convective flow and heat transfer of a suspension of Nano Encapsulated Phase Change Materials (NEPCMs) in an enclosure is studied. NEPCM particles are core-shell structured with Phase Change Material (PCM) as the core. The enclosure is a square cavity with top and bottom insulated walls and differentially-heated isothermal vertical walls. The NEPCM particles circulate under natural convection inside the cavity. The PCM cores undergo phase change from solid to liquid and absorb some of the surrounding's heat in the form of latent heat in the hot region, and release the absorbed heat in the cold region by solidification. The governing equations representing the conservation of mass, flow, and heat of NEPCM suspension are introduced in the form of partial differential equations. The governing equations are transformed into non-dimensional form and solved by the finite element method. A grid check and validation test are performed to ensure the accuracy of the results. The outcomes show that the fusion temperature of NEPCM particles is the key factor affecting the heat transfer enhancement of NEPCMs in the natural convection flow. The enhancement of heat transfer is highly dependent on the non-dimensional fusion temperature, θ_f, and very good performance can be achieved in the range of $¼ < \theta_f < ¾$. Comparing to the base fluid, a relative enhancement of about 10% can be achieved by using NEPCMs at a non-dimensional fusion temperature of ¼.

1. Introduction

Nano-Encapsulated Phase Change Materials (NEPCMs) can be considered as a new type of nanofluids, in which the nanoparticle consists of a core and a shell. The core part is made of a Phase Change Material (PCM) which can undergo a solid-liquid phase change at a certain fusion temperature, and absorb/release a significant amount of energy due to the latent heat of the phase change [1]. Literature review shows that there are various types of NEPCM suspensions. For example, Fang et al. [2] synthesized n-tetradecane as a core and formaldehyde as a polymer shell. Qiu et al. [3] prepared a sample of NEPCM with n-octadecane as the core and methylmethacrylate (MMA)-based polymer as the shell. Recently, Jamekhorshid et al. [4] and Su et al. [1] performed excellent reviews on nano/micro capsulation of phase change materials.

From a thermal-application point of view, there are various devices that are sensitive to non-uniform temperature gradients or temperature rises, such as laser optical alignment systems, computer chipsets, and detectors that demand accurate temperature control within a limited temperature range. Indeed, the temperature difference across a device may result in internal thermal stress in the sensitive structures of the device due to the mismatch of the coefficient of thermal expansion among different construction materials. Therefore, NEPCMs are promising in terms of their potential to improve the performance of working fluids, maintaining the device at a certain cooling temperature.

PCMs and nano-enhanced PCMs have been the subject of various engineering applications, particularly for thermal energy storage applications [5]. For instance, PCMs have been utilized for thermal management of buildings [6], part of walls and roofs [7], domestic heat pump and air-conditioning systems [8], and other applications including space instruments, electronic cooling devices, and the food industry [5]. Although PCMs are capable of storing/releasing a tremendous amount of energy on phase change, they are inherently very weak in terms of heat transfer. Thus, many

* Corresponding authors at: School of Aeronautic Science and Engineering, Beihang University, Beijing, PR China.
E-mail addresses: m.ghalambaz@gmail.com (M. Ghalambaz), d.wen@buaa.edu.cn, d.wen@leeds.ac.uk (D. Wen).

https://doi.org/10.1016/j.ijheatmasstransfer.2019.04.037
0017-9310/

Nomenclature

Latin letters

Cp	specific heat in constant pressure (J/kg K)
Cr	the heat capacity ratio
f	the non-dimensional fusion function defined by Eq. (23)
g	gravitational acceleration (m/s^2)
H	cavity size
h	thermal convective coefficient (W/m^2 K)
k	thermal conductivity coefficient (W/m K)
Nc	conductivity parameter
Nu	Nusselt number
Nv	viscosity parameter
p	pressure (Pa)
P	non-dimensional pressure
Pr	Prandtl number
Ra	Rayleigh number
S	dimensionless stream function
Ste	Stefan number
T	temperature (°C)
T_{Mr}	phase-change temperature range $T_{Mr} = T_2 - T_1$ (°C)
u	velocity component in x-direction (m/s)
U	non-dimensional velocity component in x-direction
v	velocity component in y-direction (m/s)
V	non-dimensional velocity component in y-direction
x	Cartesian coordinate in horizontal direction (m)
X	non-dimensional Cartesian coordinate in horizontal direction
y	Cartesian coordinate in vertical direction (m)
Y	non-dimensional Cartesian coordinate in vertical direction
ι	core-shell weight ratio

Greek symbols

μ	thermal viscosity (kg s/m)
α	thermal diffusivity (m^2/s)
β	thermal expansion coefficient (1/K)
δ	non-dimensional parameter of fusion range
θ	non-dimensional temperature
λ	ratio of the heat capacity of the NEPCM nanoparticles to the base fluid
ρ	density (kg/m^3)
ϕ	volume fraction of NEPCM nanoparticles
ψ	stream function

Subscript

b	bulk properties of the suspension
c	cold wall
c	core of NEPCM particle
f	base fluid, fusion property
h	hot wall
l	liquid phase of NEPCM cores
p	NEPCM nanoparticles
s	shell of NEPCM particle
y	local property

researchers have tried to enhance the heat transfer characteristics of PCM by using fins [9,10] or porous media [11]. There is also a number of studies that have utilized nanoparticles to enhance the heat transfer and phase change of PCMs [6,12,13]. Sometimes, nanoparticles used for enhancing the heat transfer of PCMs is abbreviated as Nano-Enhanced Phase Change Materials (NEPCMs) [12,14–16]. In such studies [12,14–16], the solid nanoparticles are added to PCM as additives to enhance the heat transfer characteristics of the medium. In contrast, in nano-encapsulation of phase change materials, the PCMs are encapsulated in a nanometer-size capsule shell, and later these particles are dispersed into a working fluid.

Many studies have modeled and simulated the natural convection of a suspension of nanoparticles in a base fluid (nanofluids) in enclosures. Hashim et al. [17] and Asabery [18] analyzed the flow and heat transfer of nanofluids in a wavy wall cavity. Sivaraj and Sheremet [19] studied the natural convection of nanofluids in a cavity with a hot plate obstacle. Ghalambaz et al. [20] and Tahmasebi et al. [21] investigated the effect of the presence of a layer of porous media and a layer of a solid wall on the flow and natural convection heat transfer of nanofluids. The effect a magnetic field [22], and conjugate heat transfer effects [23] on natural convection heat transfer in enclosures were also examined in recent studies. In all of these studies, the nanoparticles were uniform solid particles without phase-change cores.

When we consider the phase-change heat transfer of nano-encapsulated PCMs, most of the available studies are limited to forced convection heat transfer in tubes, ducts or microchannels. For instance, Seyf et al. [24] theoretically addressed the heat transfer of a slurry of 100 nm NEPCM particles-water in a channel over a square cylinder. The core of nanoparticles was made of n-octadecane. In another study, Seyf et al. [25] numerically studied the flow and heat transfer of NEPCMs in a microtube heat sink. The NEPCM was made of octadecane as core and polyalphaolefin (PAO) as the shell. They reported that the presence of nanoparticles notably improves the cooling power of the working fluid, with the cost of a tremendous pressure drop across the tube. In an experimental study, Ho et al. [26] examined the pressure drop and heat transfer enhancement resulting from using encapsulated phase-change particles in a microchannel. The results indicated that the heat transfer enhancement depended on various parameters. In some special cases, heat transfer can be boosted up to 52%, and in some cases, however, a decrease of heat transfer may be observed. Ho et al. [27,28] performed an experiment to compare the heat transfer enhancement of using either simple alumina nanoparticles or a slurry of phase-change particles in minichannels [28] and tubes [27]. It was found that various parameters, such as flow rate and the location of heating, can change the performance of heat transfer, and no general conclusion can be made.

The literature review shows that there have been some experimental and theoretical studies on forced convection of NEPCMs. However, to the best of the author's knowledge, there is no existing study on the natural convection of nano-encapsulated phase change materials, an area of high importance to future thermal control systems. The present study is the first study on modeling and simulating the natural convective behavior of NEPCMs in a cavity.

2. Mathematical model

2.1. Physical model

A square cavity of size H is filled with a suspension of nano-encapsulated phase change particles, well dispersed in the base liquid. A schematic view of the physical model and the coordinate system is depicted in Fig. 1. As seen, the left wall of the cavity is hot at the isothermal temperature of T_h, and the right wall is cold at the isothermal temperature of T_c. The top and bottom walls are well insulated. Due to the temperature difference, there is a clockwise

natural convection flow in the cavity. The nano-encapsulated PCM is made of a phase-change material as the core and a shell as the encapsulation material. The core undergoes a phase change at the fusion temperature of T_f where $T_h < T_f < T_c$. The core of NEPCM nanoparticles can phase change to liquid within its fusion temperature, and absorb/release its energy in the form of latent heat.

To model the heat transfer behavior of NEPCMs in natural convection, some assumptions are required. Here, it is assumed that the mixture of NEPCMs and a base fluid is uniform and stable. The temperature differences in the cavity are small, and thermophysical properties are independent of temperature, except for density, which is modeled by the Boussinesq approximation. It is also assumed that the nanoparticles and the base fluid are in local thermal equilibrium and that the flow is steady and incompressible.

Following [29,30] and applying some modification, the governing equations for continuity of the mixture, momentum in x and y directions and the heat conservation of the mixture by some modifications can be written as:

$$\frac{\partial u}{\partial x}+\frac{\partial v}{\partial y}=0, \tag{1}$$

$$\rho_b\left(u\frac{\partial u}{\partial x}+v\frac{\partial u}{\partial y}\right)=-\frac{\partial p}{\partial x}+\mu_b\left(\frac{\partial^2 u}{\partial x^2}+\frac{\partial^2 u}{\partial y^2}\right)+g\rho_b\beta_b(T-T_\infty) \tag{2a}$$

$$\rho_b\left(u\frac{\partial v}{\partial x}+v\frac{\partial v}{\partial y}\right)=-\frac{\partial p}{\partial y}+\mu_b\left(\frac{\partial^2 v}{\partial x^2}+\frac{\partial^2 v}{\partial y^2}\right) \tag{2b}$$

$$(\rho Cp)_b\left(u\frac{\partial T}{\partial x}+v\frac{\partial T}{\partial y}\right)=k_p\left(\frac{\partial^2 T}{\partial x^2}+\frac{\partial^2 T}{\partial y^2}\right) \tag{3}$$

where u and v are the velocities in x and y directions. Here, P is the mixture pressure, and T is the mixture temperature. The symbols of β, ρ, Cp, μ, and k here denote the volume thermal expansion, the density, the specific thermal capacity, the dynamic viscosity and the thermal conductivity of the mixture, respectively. The subscript of b denotes the bulk properties of the suspension. Finally, g indicates the gravitational constant. Based on the model description and the schematic model of Fig. 1, the boundary conditions for heat and flow are introduced as:

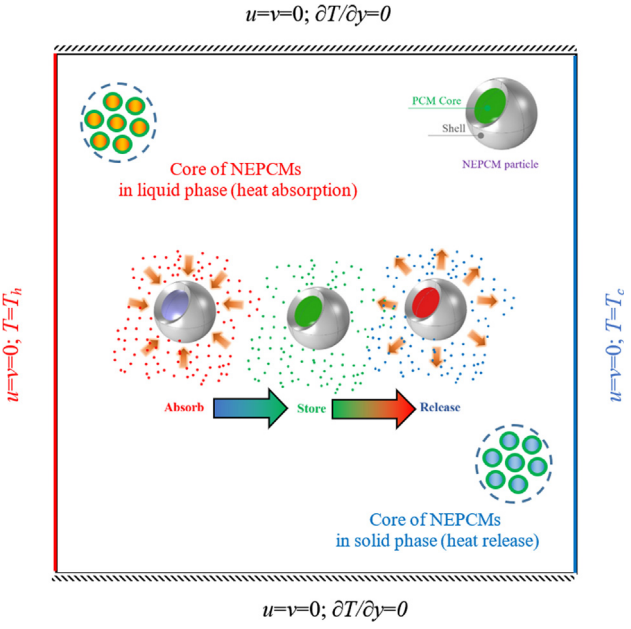

Fig. 1. Schematic view of the physical model and coordinate system.

At the hot wall $x=0$, $u=0$, $v=0$, $T=T_h$ (4a)

At the cooled wall $x=H$, $u=0$, $v=0$, $T=T_c$ (4b)

At the bottom wall $y=0$, $u=0$, $v=0$, $\partial T/\partial y=0$ (4c)

At the top wall $y=H$, $u=0$, $v=0$, $\partial T/\partial y=0$ (4d)

The top left corner of the cavity was selected as the pressure reference point, with zero relative pressure.

2.2. Bulk properties of a suspension

Based on the governing equations of Eqs. (1)–(3), the required mixture thermophysical properties are the density, the heat capacity of the mixture, the thermal volume expansion, the thermal conductivity, and the dynamic viscosity. The density of the mixture can be evaluated using the density of the NEPCM particles and the base fluid, as [31]:

$$\rho_b=(1-\phi)\rho_f+\phi\rho_p \tag{5}$$

where ϕ denotes the volume fraction of NEPCM particles, and ρ indicates the density. The subscripts of p and f represent the NEPCM nanoparticles and the base fluid.

As the nano-encapsulated phase-change particles are synthesized as a core and a shell [31,32], the effective density of these particles can be evaluated as [31,33]:

$$\rho_p=\frac{(1+\imath)\rho_c\rho_s}{\rho_s+\imath\rho_c} \tag{6}$$

where the subscript of s and c denote the shell and the core, respectively. $\imath$ is the core-shell weight ratio. It is worth noticing that the density of the liquid core PCM and the solid core PCM can be different. Here, the density of the core is approximated as the average density of the liquid and the solid phase of PCM.

Based on the energy equation and considering the thermal equilibrium between the nanoparticles and the base fluid, Khanafer and Vafai [34] proposed the following relation for calculating the specific heat capacity of a mixture:

$$Cp_b=\frac{(1-\phi)\rho_f Cp_f+\phi\rho_p Cp_p}{\rho_b} \tag{7}$$

The overall specific heat capacity of an encapsulated nanoparticle, consisting of a core and a shell with no change phase, can be evaluated as [33]:

$$Cp_p=\frac{(Cp_{c,l}+\imath Cp_s)\rho_c\rho_s}{(\rho_s+\imath\rho_c)\rho_p} \tag{8}$$

Here, it should be noticed that the specific heat capacity of the core in the liquid phase can be different from that of the solid phase. Hence, the specific heat capacity of the core PCM is approximated as the average of the liquid and solid heat capacity of the PCM, which is indicated by the subscript of c,l. In the present study, the core PCM undergoes a phase change, and hence, the latent heat of change phase should be taken into account as a part of the

specific heat of the NEPCM particles. A rectangular, triangular or sine profile can be used to model the latent heat of phase change as a part of the specific heat of the core PCM when it undergoes a phase change [25,31]:

$$Cp_c = Cp_{c,l} + \frac{h_{sf}}{T_{Mr}} \tag{9a}$$

$$Cp_c = Cp_{c,l} + \left\{\frac{\pi}{2}\cdot\left(\frac{h_{sf}}{T_{Mr}} - Cp_{c,l}\right)\cdot \sin\left(\pi\frac{T-T_1}{T_{Mr}}\right)\right\} \tag{9b}$$

$$Cp_c = Cp_{c,l} + 2\left(\frac{h_{fs}}{T_{Mr}^2} - \frac{Cp_{c,l}}{T_{Mr}}\right)(T-T_1) \tag{9c}$$

In fact, instead of a fixed fusion temperature of T_f, which results in a discontinuity in the heat equation, it is assumed that the phase change occurs in a small temperature interval (T_{Mr}) with the fusion temperature of T_f in its middle to avoid the discontinuity in the heat equation. If T_{Mr} tends to zero, the exact fusion temperature of T_f can be recovered. When the core temperature is lower than the melting range, $T < (T_f - T_{Mr}/2)$, the core is in the solid phase. For temperatures higher than the melting range, $T < (T_f + T_{Mr}/2)$, the core is in the liquid phase. When the core temperature is within the melting range, it is partially molten, and its specific heat capacity including the latent heat can be evaluated using each one of Eqs. (9a)–(9c).

Alisetti and Roy [35] addressed the effect of using different phase-change heat-capacity profiles on the heat transfer of a slurry of microphase change particles in a circular pipe. They reported that the difference is less than 4%. We selected the sine profile to represent the heat capacity of the NEPCM core due to its numerical advantages. Indeed, using the sine profile significantly enhances the numerical convergence by smoothing the changes in the specific heat capacity of the NEPCM core. By taking into account the sensible and latent heat of the phase change, the total specific heat capacity of the PCM core can be written as:

$$Cp_c = Cp_{c,l} + \left\{\frac{\pi}{2}\cdot\left(\frac{h_{sf}}{T_{Mr}} - Cp_{c,l}\right)\cdot \sin\left(\pi\frac{T-T_1}{T_{Mr}}\right)\right\}\begin{cases} 0 & T < T_f - T_{Mr}/2 \\ 1 & T_f - T_{Mr}/2 < T < T_f + T_{Mr}/2 \\ 0 & T > T_f + T_{Mr}/2 \end{cases} \tag{10}$$

Now, by substituting Eq. (10) in Eq. (8), the overall specific heat capacity of the NEPCM particle including the shell and the core can be obtained. The thermal volume expansion of the mixture of nanoparticles and base fluid can be modeled as a superposition of the thermal expansion of the fluid and the nanoparticles. Following the study of Khanafer and Vafai [34], the thermal volume expansion of the mixture of nanoparticles and a base fluid, β_b, can be evaluated as:

$$\beta_b = (1-\phi)\beta_f + \phi\beta_p \tag{11}$$

In the case of micro-encapsulated PCMs, the literature review shows that the shear rate induces a significant effect on the apparent thermal conductivity of the slurry of microparticles and base fluid. Hence, for micro PCMs, the thermal conductivity was divided into two parts, static thermal conductivity and dynamic thermal conductivity. The static thermal conductivity part is usually evaluated by the well-known Maxwell model [34]. The dynamic part of the thermal conductivity is a function of shear rate, as discussed in [25,29,31]. Indeed, the microparticles are large enough to be affected by the velocity difference along with the particle. In contrast, at the nanoscale, the particles are too fine to be affected by regular shear rates in the fluid flow [36]. Thus, the thermal conductivity relations for the mixture of MEPCMs are inadequate for NEPCMs.

Buongiorno [37] and Venerus et al. [38] have performed two important benchmark studies on the thermal conductivity and dynamic viscosity of nanofluids. The experiments on the synthesis and measurement of the thermal conductivity and dynamic viscosity of a suspension of nanoparticles and a base fluid were carried out by different scientists in different laboratories. The results of these benchmark experiments reveal that there is a linear relationship between the thermal conductivity of the suspension of nanoparticles and the volume fraction of the nanoparticles. In the case of dynamic viscosity, as well, a linear relationship between the dynamic viscosity and the volume fraction of the nanoparticles was confirmed. Thus, Zaraki et al. [39] and Ghalambaz et al. [12] employed the following linear relations to model the thermal conductivity and dynamic viscosity of a suspension of nanoparticles and a base fluid:

$$\frac{k_b}{k_f} = 1 + Nc\phi \tag{12a}$$

$$\frac{\mu_b}{\mu_f} = 1 + N\nu\phi \tag{12b}$$

where Nc denotes the number of thermal conductivity, and Nv denotes the number of dynamic viscosity. As seen, the larger the values of Nc and Nv, the larger the increase in the thermal conductivity and dynamic viscosity of the suspension by the presence of nanoparticles.

Indeed, the number of thermal conductivity (Nc) and the number of dynamic viscosity (Nv) can be changed by altering various parameters, such as the size of the nanoparticles, the shape of the nanoparticles, the type of the nanoparticles, and the type of the base fluid. They can also be a function of the preparation method, the temperature of the suspension, the type and volume fraction of additives, ultrasonication time or other parameters. However, Nc and Nv are constant for a synthesized nanofluid, and they represent the sensitivity of the suspension to a change in the volume fraction of the nanoparticles. The values of Nc and Nv for some nanofluids and hybrid nanofluids have been evaluated and reported in [12,39].

The relations of Eq. (12) are only applicable for low volume fractions of nanoparticles ($\phi < 5\%$), and they cannot be employed for a slurry of nanoparticles. By assuming a dilute suspension of NEPCMs, Eqs. (12a) and (12b) are employed to evaluate the thermal conductivity and dynamic viscosity of the mixture.

2.3. Non-dimensional form of governing equations

Invoking the following dimensionless parameters, the governing Eqs. (1)–(3) and the corresponding boundary conditions Eq. (4) can be written into a non-dimensional form:

$$X = \frac{x}{H},\quad Y = \frac{y}{H},\quad U = \frac{uH}{\alpha_f},\quad V = \frac{\nu H}{\alpha_f},\quad P = \frac{pH^2}{\rho_f\alpha_f^2},\quad \theta = \frac{T-T_c}{T_h-T_c} \tag{13a}$$

Accordingly, the non-dimensional parameters can be introduced in the following form:

$$Ra = \frac{g\rho_f\beta_f(T_h-T_c)H_3}{\alpha_f\mu_f},\quad Pr = \frac{\mu_f}{\rho_f\alpha_f} \tag{13b}$$

where Ra and Pr represent the Rayleigh and Prandtl numbers, respectively. Upon substituting Eqs. (13) into Eqs. (1)–(3), the governing equations can be rewritten in dimensionless form as follows:

$$\frac{\partial U}{\partial X}+\frac{\partial V}{\partial Y}=0, \tag{14}$$

$$\left(\frac{\rho_b}{\rho_f}\right)\left(U\frac{\partial U}{\partial X}+V\frac{\partial U}{\partial Y}\right)=-\frac{\partial P}{\partial X}+Pr\left(\frac{\mu_b}{\mu_f}\right)\left(\frac{\partial^2 U}{\partial X^2}+\frac{\partial^2 U}{\partial Y^2}\right) \tag{15a}$$

$$\left(\frac{\rho_b}{\rho_f}\right)\left(U\frac{\partial V}{\partial X}+V\frac{\partial V}{\partial Y}\right)=-\frac{\partial P}{\partial Y}+Pr\left(\frac{\mu_b}{\mu_f}\right)\left(\frac{\partial^2 V}{\partial X^2}+\frac{\partial^2 V}{\partial Y^2}\right)+RaPr\left(\frac{\beta_b}{\beta_f}\right)\theta \tag{15b}$$

$$\frac{(\rho Cp)_b}{(\rho Cp)_f}\left(U\frac{\partial \theta}{\partial X}+V\frac{\partial \theta}{\partial Y}\right)=\left(\frac{k_b}{k_f}\right)\left(\frac{\partial^2 \theta}{\partial X^2}+\frac{\partial^2 \theta}{\partial Y^2}\right) \tag{16}$$

Here, the term of $(Cp_b\rho_b)/(Cp_f\rho_f)$ shows the heat capacity ratio (Cr). The parameter Cr represents the heat capacity of the mixture (the sensible and latent heat of phase change) to the sensible heat capacity of the base fluid.

2.4. Non-dimensional form of boundary conditions

The non-dimensional boundary conditions are as follows:

At the hot wall $X=0,\quad U=0,\quad V=0,\quad \theta=1$ (17a)

At the cooled wall $X=1,\quad U=0,\quad V=0,\quad \theta=0$ (17b)

At the bottom wall $Y=0,\quad U=0,\quad V=0,\quad \partial\theta/\partial Y=0$ (17c)

At the hot wall $Y=1,\quad U=0,\quad V=0,\quad \partial\theta/\partial Y=0$ (17d)

By substituting the thermophysical properties models of Eqs. (5)–(11), the non-dimensional governing equations of (14)–(16) can be simplified and rewritten as:

$$\frac{\partial U}{\partial X}+\frac{\partial V}{\partial Y}=0, \tag{18}$$

$$\left((1-\phi)+\phi\frac{\rho_p}{\rho_f}\right)\left(U\frac{\partial U}{\partial X}+V\frac{\partial U}{\partial Y}\right)=-\frac{\partial P}{\partial X}+Pr(1+N\nu\phi)\left(\frac{\partial^2 U}{\partial X^2}+\frac{\partial^2 U}{\partial Y^2}\right) \tag{19a}$$

$$\left((1-\phi)+\phi\frac{\rho_p}{\rho_f}\right)\left(U\frac{\partial V}{\partial X}+V\frac{\partial V}{\partial Y}\right)=-\frac{\partial P}{\partial Y}+Pr(1+N\nu\phi)\left(\frac{\partial^2 V}{\partial X^2}+\frac{\partial^2 V}{\partial Y^2}\right)+RaPr\left((1-\phi)+\phi\frac{\beta_p}{\beta_f}\right)\theta \tag{19b}$$

$$Cr\times\left(U\frac{\partial \theta}{\partial X}+V\frac{\partial \theta}{\partial Y}\right)=(1+Nc\phi)\left(\frac{\partial^2 \theta}{\partial X^2}+\frac{\partial^2 \theta}{\partial Y^2}\right) \tag{20}$$

where θ_f is the non-dimensional fusion temperature, λ is the sensible heat capacity ratio, and δ is the non-dimensional melting interval. These non-dimensional parameters are defined as:

$$\theta_f=\frac{T_f-T_c}{T_w-T_c}\quad \delta=\frac{T_{Mr}}{T_w-T_c},\ \lambda=\frac{(Cp_{c,l}+\imath Cp_s)\rho_c\rho_s}{(\rho Cp)_f(\rho_s+\imath\rho_c)} \tag{21}$$

Using Eqs. (7)–(10), the term of the heat capacity ratio, Cr, can be written as:

$$\frac{Cp_b\rho_b}{Cp_f\rho_f}=(1-\phi)+\phi\frac{(Cp_{c,l}+\imath Cp_s)\rho_c\rho_s}{Cp_f(\rho_s+\imath\rho_c)\rho_f}+\phi\frac{(T_w-T_C)}{T_{Mr}}\left\{\frac{\pi\rho_c\rho_s}{2Cp_f(\rho_s+\imath\rho_c)\rho_f}\left(\frac{h_{sf}-Cp_{c,l}T_{Mr}}{(T_w-T_C)}\right)\right\}f \tag{22}$$

where f is the non-dimensional fusion function defined as

$$f=\frac{\pi}{2}\sin\left(\frac{\pi}{\delta}\left(\theta-\theta_f+\frac{\delta}{2}\right)\right)\times\begin{cases}0 & \theta<\theta_f-\frac{\delta}{2}\\ 1 & \theta_f-\frac{\delta}{2}<\theta<\theta_f+\frac{\delta}{2}\\ 0 & \theta>\theta_f+\frac{\delta}{2}\end{cases} \tag{23}$$

In Eq. (22), the term $\left[(\rho_c\rho_s)(h_{sf}-Cp_{c,l}T_{Mr})\right]/\left[(T_w-T_C)\left(Cp_f(\rho_s+\imath\rho_c)\rho_f\right)\right]$ represents the combination of latent heat and sensible heat. T_{Mr} indicates the interval temperature of the phase change, which is a very small interval. Moreover, it should be noted that the sensible heat, $Cp_{c,l}$, is very small compared to the latent heat. Hence, the term of $Cp_{c,l}\times T_{Mr}$ can be neglected, and hence, the Stefan number can be introduced in the usual way as:

$$Ste=\frac{(\rho Cp)_f(T_w-T_c)(\rho_s+\imath\rho_c)}{(h_{sf}\rho_c\rho_s)} \tag{24}$$

Consequently, Cr can be introduced in the form of non-dimensional parameters as:

$$C_r=\frac{Cp_b\rho_b}{Cp_f\rho_f}=(1-\phi)+\phi\lambda+\frac{\phi}{\delta Ste}f \tag{25}$$

Using Eq. (25), Eq. (20) can be re-written as:

$$\left((1-\phi)+\phi\lambda+\frac{\phi}{\delta Ste}f\right)\left(U\frac{\partial \theta}{\partial X}+V\frac{\partial \theta}{\partial Y}\right)=(1+Nc\phi)\left(\frac{\partial^2 \theta}{\partial X^2}+\frac{\partial^2 \theta}{\partial Y^2}\right) \tag{26}$$

The characteristic parameter of heat transfer in the present study is the Nusselt number. This parameter indicates the rate of heat transfer in the cavity. The balance of thermal conduction and convection at the hot/cold wall of the cavity can be written as:

$$\text{Hot wall}: -k_b\left.\frac{\partial T}{\partial y}\right|_{x=0}=h(T_w-T_c),\ \text{and}$$
$$\text{Cold wall}: -k_b\left.\frac{\partial T}{\partial y}\right|_{x=1}=h(T_w-T_c) \tag{27}$$

By employing the non-dimensional variables of Eq. (13), Eq. (27) is re-written as:

$$\text{Hot wall}: Nu_y=-\frac{k_b}{k_f}\frac{\partial\theta}{\partial X}\Big)_{X=0},\ \text{and Cold wall}: Nu_y=-\frac{k_b}{k_f}\frac{\partial\theta}{\partial X}\Big)_{X=1} \tag{28}$$

where $Nu_y = h_yH/k$. Substituting the thermal conductivity ratio from Eq. (12a), the local Nusselt number is achieved as:

$$\text{Hot wall}: Nu_y=-(1+Nc\phi)\frac{\partial\theta}{\partial X}\Big)_{X=0}\quad\text{and}$$
$$\text{Cold wall}: Nu_y=-(1+Nc\phi)\frac{\partial\theta}{\partial X}\Big)_{X=1} \tag{29}$$

Finally, the average Nusselt number is introduced at the hot wall as:

$$Nu = -(1 + Nc\phi)\int_0^1 \frac{\partial\theta}{\partial X}\Big)_{X=0} dY \tag{30}$$

It should be noted that in the case of steady-state flow and heat transfer, the average Nusselt number at the hot wall is identical with the average Nusselt number at the cold wall. Hence, here only the average Nusselt number at the hot wall is introduced and adopted as the average Nusselt number.

3. Numerical method and code validation

The finite element method is utilized to numerically solve the non-dimensional governing equations of (19), (26) and (28) associated with the boundary conditions Eq. (17). The governing equations are written in the weak form, and discretized over a non-uniform structure grid to be solved using the Galerkin finite element method. The governing equations for the fluid flow and the heat transfer are fully coupled by applying the damped Newton method. Then, the Parallel Sparse Direct Solver is employed to solve the algebraic set of equations. The iterations are repeated until the residuals reach below 10^{-5}. The details of this method are discussed in [40].

The grid of this study is a structured non-uniform grid. A schematic view of the utilized grid is depicted in Fig. 2. As seen, the grid points near the walls are denser to accurately capture high gradients of the velocity and temperature next to the walls. The number of grids in the horizontal (m) and vertical (n) directions are equal, where the grid size is denoted by $m \times n$. In order to ensure the accuracy of the results, the effect of the grid size on the calculations is studied by repeating the calculations for various grid sizes. The default values of the non-dimensional parameters are adopted as $Ste = 0.313$, $\lambda = 0.4$, $Pr = 6.2$, $\rho_p/\rho_f = 0.9$, of $\phi \times \beta_p/\beta_f = 0$ and $Nc = Nv = 3.0$, which will be discussed later in more detail in the results section.

The selection of an adequate value of the non-dimensional melting range δ is an important step in performing the numerical calculations. A large value of δ may result in non-realistic solutions as the phase change of tiny NEPCM particles occurs in temperature near the fusion temperature. Selecting a very small value of δ would result in numerical convergence problems by inducing a large sudden variation in the heat capacity of the mixture. In order to find an adequate value of δ, the case of a high Rayleigh number of $Ra = 10^6$ is adopted. The calculations were performed with various values of δ in the range of 0.015–0.1, and the average Nusselt number was monitored. Based on the outcomes, only a 0.04% change in the average Nusselt number was observed by variation of δ in the mentioned range. Furthermore, the case of a low Rayleigh value of 10^4 was checked, and the average Nusselt number was monitored for the same range of δ. The outcomes show that the variation of δ only changes the average Nusselt number by 0.07%.

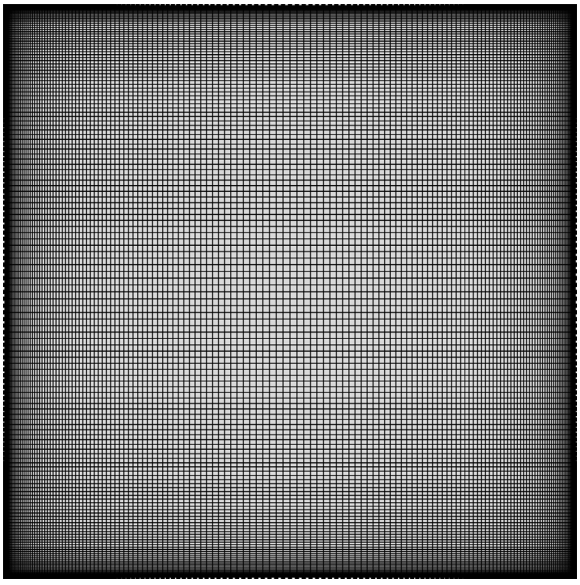

Fig. 2. View of the utilized grid with a size of 150 × 150 and a stretching ratio of 10.

The computational time for small values of δ increases dramatically due to the pulse behavior of the thermal capacity of the mixture. It should be noted that selecting a too-small value of δ requires a very fine mesh to be captured. Hence, $\delta = 0.05$ is adopted for the sake of accuracy and computational costs.

It is worth mentioning that the heat equation was discretized using quadrature elements, which significantly increases the accuracy of the results. The quadrature discretization was adopted due to the phase change inherent in NEPCMs in a small range. The largest Rayleigh number of this study, $Ra = 10^6$, is selected to check the grid. Increasing the Rayleigh number boosts the buoyancy effects, and as a result, the temperature and velocity gradients next to the walls increase. Hence, the grid check analysis is performed for a large Rayleigh number to ensure the accuracy of all of the results. Table 1 shows the average Nusselt number and maximum velocity of the fluid inside the cavity for various grid sizes. As seen, the grid size of 150 × 150 shows good accuracy up to two significant digits for the average Nusselt number. Using the grid size of 150 × 150 corresponds to about 0.01% relative error in average Nusselt number and about 0.08% relative error in maximum velocity compared to the very fine grid of 400 × 400. A relative error below 1% is excellent for most engineering applications and graphical demonstration of the results. Hence, to maintain sufficient accuracy and reasonable computational costs, the grid size of 150 × 150 is adopted for all the calculations in the present study.

In order to check the robustness of the utilized code and the correctness of the results, the outcomes are compared with the available literature results in some possible cases. In the first comparison, the results are compared with the results of Turan et al. [41] for a square cavity with differentially-heated side walls and insulated top and bottom walls which was filled with a non-Newtonian power-law fluid. Considering the power law index as unity in the study of Turan et al. [41], and assuming zero volume fraction of nanoparticles in the present study, the governing equations for both studies are identical, and the results can be compared. The comparison between the non-dimensional temperature profiles of [41] and the present study is depicted in Fig. 3 when $Ra = 10^5$ and $Pr = 1000$. The average Nusselt number in [41] was reported as 9.20; here it is calculated as 9.23. The maximum vertical velocity in a horizontal line at the center of the cavity was reported as 235.96 in [41]. In the present study, it is calculated as 236.08. As seen, there is a very good agreement between the results of the two studies for the temperature profiles, maximum vertical velocity, and calculated average Nusselt number.

In the second comparison, the study of Kahveci [42] is selected. Kahveci [42] addressed the natural convection heat transfer of nanofluids in a tilted cavity. Assuming zero tilted angle in [42] and neglecting the phase change effects in the present study (simple solid nanoparticles with no phase change), the physics of the two studies are almost the same. However, in [42] the Maxwell model for thermal conductivity and the Brinkman model for viscosity were utilized. Using curve-fitting on the Maxwell and Brinkman models, the number of thermal conductivity and number of

Table 1
The effect of grid size on the average Nusselt number when $Ra = 10^6$ and $\delta = 0.05$.

Grid size	100 × 100	150 × 150	200 × 200	250 × 250	300 × 300	400 × 400
Average Nu	10.124	10.128	10.127	10.126	10.127	10.127
Maximum velocity	222.82	222.71	222.87	222.92	222.91	222.90

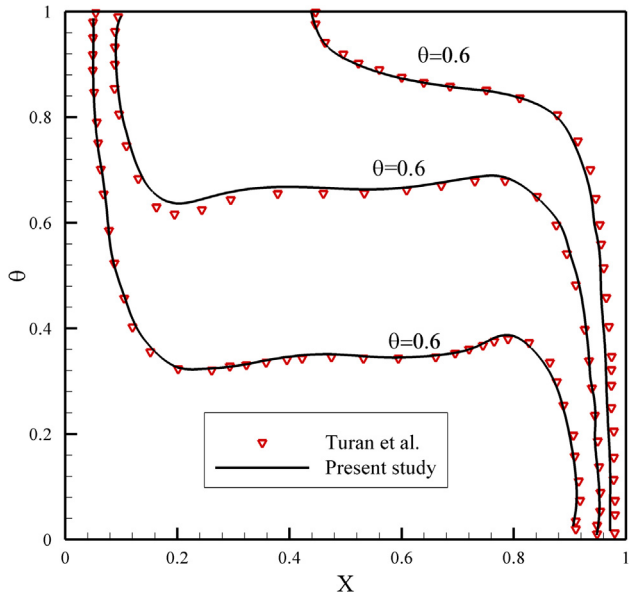

Fig. 3. Comparison between the temperature profiles of Turan et al. [41] (Newton fluid index = 1) and the results of the present study when $Ra = 10^5$ and $Pr = 1000$ (the right wall is hot and left wall is cold).

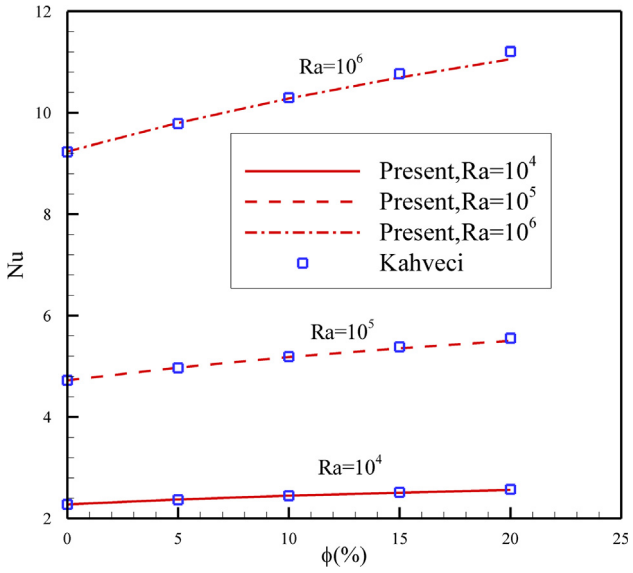

Fig. 4. Comparison between the results of Nu evaluated in the present study and those reported in the study of Kahveci [42] for the case of Al_2O_3-water nanofluid and $Pr = 6.2$.

dynamic viscosity can be approximated as $Nc = 3.3$ and $Nv = 2.88$ for water-Al_2O_3. Following the thermophysical values of [42], the comparison between the Nusselt numbers evaluated here and reported in [42] is depicted in Fig. 4. This figure depicts a very good agreement between the results of these two studies.

Finally, the evaluated average Nusselt number in the present study is compared with the literature studies when $Pr = 0.7$ and $\phi = 0$ in Table 2. This table confirms a very good agreement between the present results and those reported in the literature.

4. Results and discussion

The non-dimensional parameters in this study are the volume fraction of nanoparticles (ϕ), the Stefan number (Ste), the heat capacity ratio (λ), the fusion temperature of the NEPCM core (θ_f), the density ratio (ρ_P/ρ_f), the number of thermal conductivity (Nc), the number of dynamic viscosity (Nv), the Rayleigh number (Ra), and the Prandtl number (Pr).

The suspension of NEPCM particles and the base fluid is assumed as a dilute suspension, and hence, the volume fraction is adopted as $0 < \phi < 0.05$. Taking PMMA as the shell for the NEPCM particles [45], n-octadecane as the core PCM [46], water as the base fluid [46], and considering the core-shell weight ratio as $\iota \sim 0.7$, the Stefan number and heat capacity ratio are about 0.313 and 0.4, respectively. The non-dimensional fusion temperature can be varied in the range of cold wall temperature to the hot wall temperature as $0 < \theta_f < 1$. Following [12], the number of thermal conductivity and the number of dynamic viscosity are selected as $0 < Nc < 6$ and $0 < Nv < 6$. It should be noted that the zero values of Nc and Nv are not applicable for nanofluids. Large values of Nc and Nv (>6) are also possible for nanofluids. As the PCM core is lighter than water [47,48], and PMMA is heavier than water, the density ratio is adopted as $0.7 < \rho_P/\rho_f < 0.9$. The thermal expansion coefficient of the solid particles is much lower than that of the liquid base fluids, and the volume fraction of NEPCM particles is also low. Hence, the term $\phi \times \beta_p/\beta_f$ is negligible and assumed to be zero.

The Prandtl number for liquids is higher than unity, and here, the regular Prandtl number of water as $Pr = 6.2$ is selected. The Rayleigh number is in the range of 10^4–10^6, where the low values of Rayleigh number represent the conduction-dominant heat transfer regime and high Rayleigh numbers represent the convection-dominant heat transfer regime. Based on the grid check results, the value of the non-dimensional fusion interval, δ, was fixed as $\delta = 0.05$. Finally, the default values of the non-dimensional parameters are adopted as: (ϕ), $Ste = 0.313$, $\lambda = 0.4$, $\theta_f = 0.3$, $\rho_P/\rho_f = 0.9$, $Nc = 3.0$, $Nv = 3.0$, $Ra = 10^5$, and $Pr = 6.2$. The results of the present study are reported for these values; otherwise, the value of the non-dimensional parameter will be stated. As all of the results and parameters are in non-dimensional form, the prefix of "non-dimensional" may be omitted in some parts of the text for the sake of abbreviation.

Fig. 5 shows the effect of fusion temperature on the isotherm contours, streamlines and heat capacity ratio of the mixture to the base fluid (Cr) in the cavity for two fusion temperatures of $\theta_f = 0.3$ and $\theta_f = 0.5$. Fig. 6 depicts the local Nusselt number at the hot and cold walls of the cavity. Fig. 7(a) and (b) illustrate the average Nusselt number as a function of the fusion temperature for various values of Stefan number when $Ra = 10^5$ and $Ra = 10^6$. Indeed, Fig. 7 summarizes the heat transfer effect of fusion temperature and Stefan number on the convective heat transfer rate in the cavity.

Fig. 5(c) shows the variation of heat capacity in the cavity. Indeed, the variation of heat capacity is due to the phase change. Therefore, the red area in Fig. 5(c) depicts the region with the

Table 2
Comparison of average Nusselt number at the hot wall evaluated in the present study and those reported in the literature when $\phi = 0$ and $Pr = 0.7$.

Ra	10^3	10^4	10^5	10^6
Deng and Tang [43]	1.1180	2.2540	4.5570	–
Anandalakshmi and Tanmay [44]	1.1179	2.2482	4.5640	–
Present study	1.1174	2.2441	4.5174	8.8167

phase change. In the red region, the nano-encapsulated particles undergo phase change phase inside their capsules.

Fig. 5 reveal that changing the fusion temperature from $\theta_f = 0.3$ and $\theta_f = 0.5$ affects the distribution of temperature at the center of the cavity. The heat capacity ratio in Fig. 5 shows a ribbon shape around the constant temperature line of fusion. The capacity ratio parameter outside the fusion region is constant as 0.97, and it is variable inside the fusion temperature. The red region illustrated in the *Cr* contours of Fig. 5(a) depicts the region of phase change. The ribbon shape of the phase change area is very thin next to the wall, due to the large temperature gradients. The ribbon shape gets wider in central areas of the cavity, where the temperature gradients are smooth. The streamlines are also affected by the change of fusion temperature.

Fig. 6(a) shows that most of the differences between the local Nusselt numbers occur at the bottom of the wall. At the bottom of the hot wall, the local Nusselt number increases by the increase of fusion temperature from $\theta_f = 0.1$ to $\theta_f = 0.5$ in most cases. Attention to isotherm patterns (depicted in Fig. 5(a) and (b)) reveals that the isotherm of $\theta = 0.1$ is a line close to the cold wall with a small extension at the bottom of the cavity, then $\theta = 0.3$ is a line next to the cold wall but with a larger extension at the bottom of the cavity. The isotherm of $\theta = 0.5$ starts from the top of the cold wall and moves down vertically until y = 0.5, then it moves toward the hot wall horizontally, and then again it follows the hot wall toward its bottom vertically. As mentioned, the phase change of the NEPCM particles takes place around the isotherm identical with their fusion temperature. Moreover, a comparison between the isotherms of Fig. 5 reveals that the change of fusion temperature only slightly changes the pattern of isotherms in the cavity. Thus, it can be concluded that the increase of fusion temperature moves the phase-change phenomenon toward the bottom of the hot wall. This is where the heat flux shows a significant change by the change of the fusion temperature θ_f. In all of the three cases of $\theta_f = 0.1$, 0.3 and 0.5, the isotherms are far away from the top section of the hot wall, and hence, the local heat flux curves (local Nusselt number) at the top of the hot wall are almost identical and independent of the variation of θ_f. In the case of $\theta_f = 0.5$, a small but notable change of heat flux in the middle of the hot wall (about y = 0.5) can be seen. This is due to the behavior of isotherm departure from the cold wall. Similarly, the local Nusselt numbers follow the behavior of the isotherms identical to the fusion temperature of the NEPCMs. As seen, the differences between the local Nusselt numbers at the top of the cold wall are notable. As mentioned, the isotherms of $\theta = 0.1$–0.5 start from the top of the cold wall. This is the location of the change phase for NEPCMs with the fusion temperature in this range.

From Fig. 7, it is clear that decreasing the Stefan number increases the average Nusselt number. Indeed, as the latent heat of the PCM cores rises, the Stefan number decreases. Hence, the

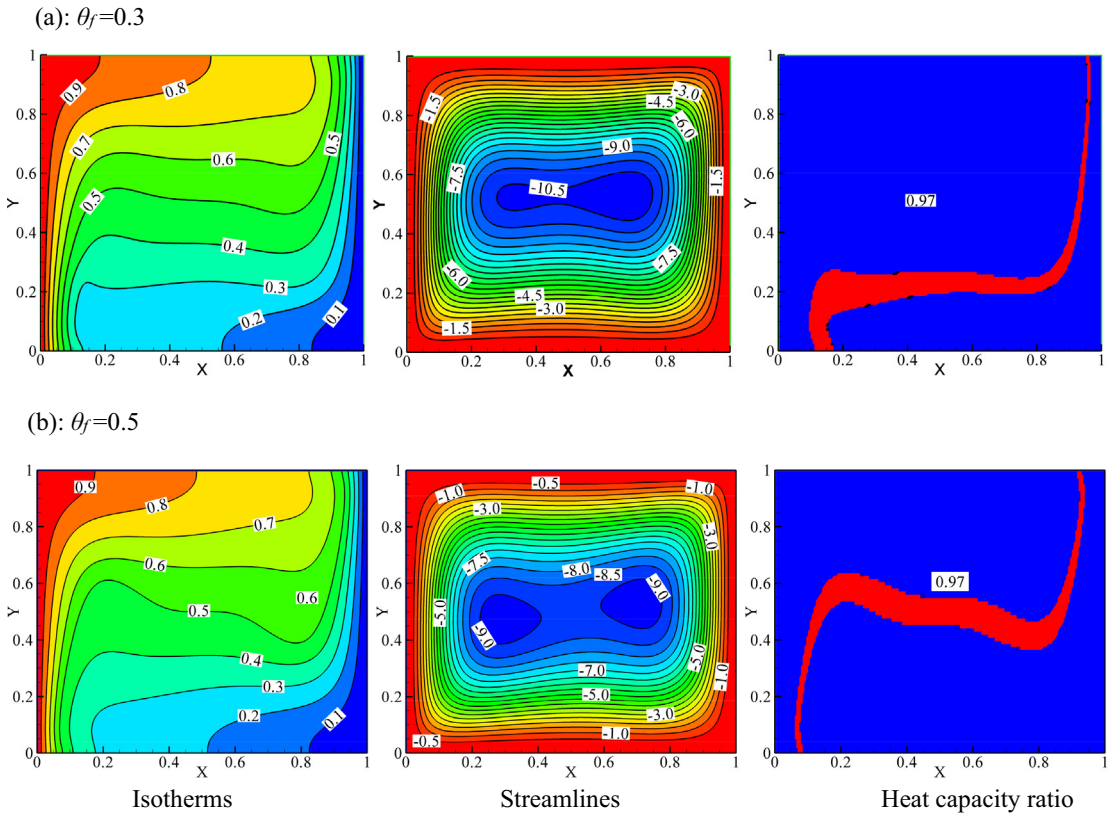

Fig 5. The isotherm contours, streamlines and *Cr* contours for two non-dimensional fusion temperatures of $\theta_f = 0.3$ and $\theta_f = 0.5$.

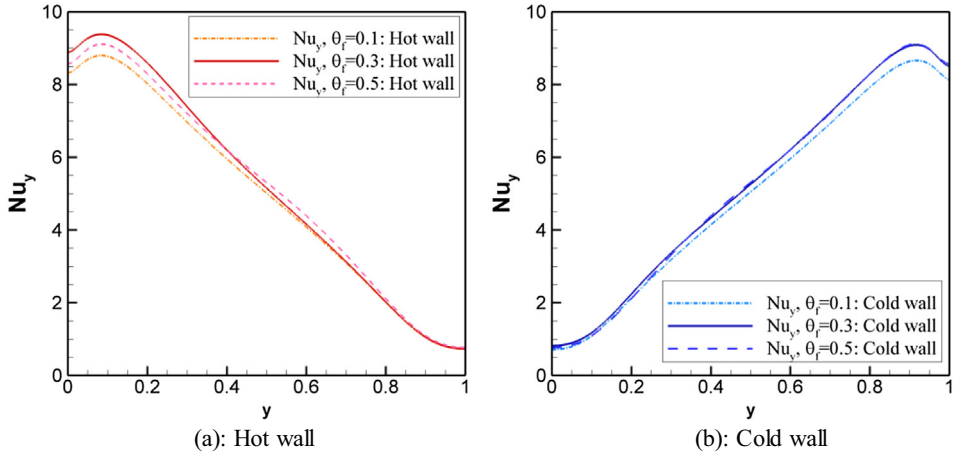

Fig. 6. Local Nusselt number at the hot wall and the cold wall for two non-dimensional fusion temperatures of $\theta_f = 0.3$ and $\theta_f = 0.5$.

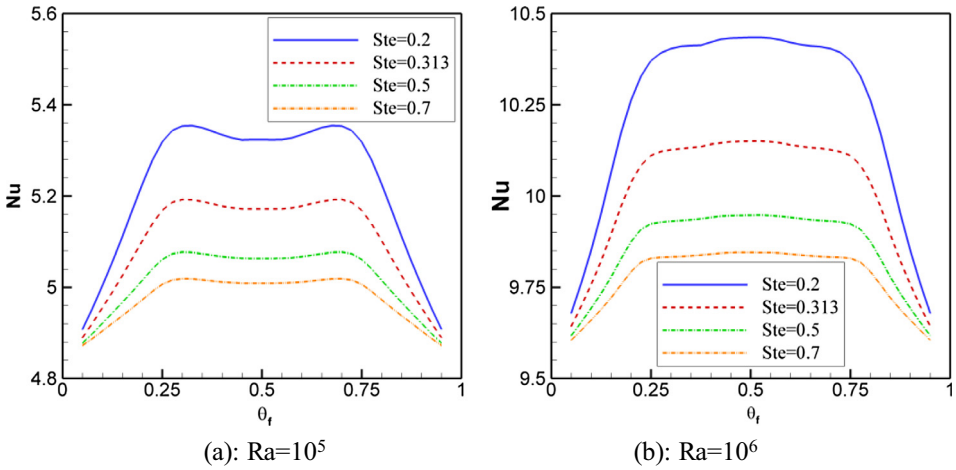

Fig. 7. The average Nusselt number as a function of non-dimensional fusion temperature (θ_f) for various values of Stefan number; (a): $Ra = 10^5$; (b): $Ra = 10^6$.

smaller the Stefan number, the larger the latent heat of the PCM cores. By the increase of the latent heat of the PCM cores, the heat storage capacity of the NEPCM particles increases, which as a result leads to a higher heat transfer rate in the cavity. The results of Fig. 7(b) demonstrate that the average Nusselt number as a function of non-dimensional fusion temperature, θ_f, shows a symmetrical behavior for $\theta_f = 0.5$. This behavior was expected, due to the symmetry of the geometry and boundary conditions. When the fusion temperature is low, the increase in the fusion temperature increases the average Nusselt number. For fusion temperatures in the range of 0.25–0.75, there is a maximum peak for average Nusselt number when the Rayleigh number is 10^6. In contrast, when the Rayleigh number is 10^5, there is a local minimum in the fusion range of 0.25–0.75. In the case of $Ra = 10^6$, the maximum average Nusselt number can be observed at the fusion temperature of 0.5. As seen in Fig. 5, when the fusion temperature is about 0.5, the middle of the cavity acts as the phase change region. The phase change region is close to both the hot and cold regions. Hence, the heat transfer is maximum. In the case of $Ra = 10^6$ and $Ste = 0.313$, the maximum Nusselt number is about 10.15, while the average Nusselt number for pure liquid is about 9.22. Hence, by using 5% of NEPCM particles and with the optimum fusion temperature of 0.5, the heat transfer can be enhanced up to 10% compared to the base fluid. This enhancement in the case of $Ste = 0.2$ can be increased up to 12.7%.

As mentioned, when the Rayleigh number is low, $Ra = 10^5$, there is a local minimum in the range of $0.25 < \theta_f < 0.75$, and the maximum heat transfer occurs at the fusion temperature about 0.25 and 0.75. In the case of $Ra = 10^5$, the average Nusselt number of pure fluid is 4.72. Considering the case of Ste = 0.313, and $\theta_f = 0.25$, the average Nusselt number can be enhanced up to 10% when $Ra = 10^5$ is in the presence of a 5% volume fraction of NEPCM particles. The analysis of the boundary layer heat transfer of nanofluids over a flat plate indicates the maximum heat transfer enhancement for the non-dimensional fusion temperature of $\theta_f = 0.25$ [49], which is in good agreement with the results of the cavity study.

It is worth mentioning that the average Nusselt numbers for the cold and hot walls are monitored, and it is found that they are identical. Identically the average Nusselt numbers at hot and cold walls are expected, due to the heat conservation law. However, from a numerical point of view, the identical average Nusselt numbers confirm that the utilized grid and the numerical technique were adequate to deal with the heat equation and the phase change non-linearities. Moreover, for a pure fluid with the Prandtl number of $Pr = 6.2$, the average Nusselt numbers are $Nu = 4.7206$

Table 3
The effect of various non-dimensional parameters on the average Nusselt number for the default case with $Ra = 10^{5.}$

Ste	θ_f	λ	ρ_p/ρ_f	*Nc*	*Nv*	*Nu*
0.313	0.3	0.4	0.9	3.0	3.0	5.1932
0.313	0.3	0.4	0.9	3.0	6.0	5.0030
0.313	0.3	0.4	0.9	6.0	3.0	5.6533
0.313	0.3	0.4	0.9	6.0	6.0	5.4477
0.313	0.3	0.4	0.7	3.0	3.0	5.1933
0.313	0.3	0.3	0.9	3.0	3.0	5.1864
0.313	0.2	0.4	0.9	3.0	3.0	5.1022
0.313	0.1	0.4	0.9	3.0	3.0	4.9550
0.2	0.3	0.4	0.9	3.0	3.0	5.3541

(when $Ra = 10^5$) and $Nu = 9.2197$ (when $Ra = 10^6$). Comparison of the average Nusselt number of a pure fluid with the magnitude of the plotted average Nusselt numbers in Fig. 7(a) and (b) demonstrates the enhancement of heat transfer (Nu) regardless of the magnitude of the non-dimensional fusion temperatures. However, using the non-dimensional fusion temperature in the range of $0.25 < \theta_f < 0.75$ would further enhance the heat transfer. Considering the default case of $Ste = 0.313$, using NEPCMs with the appropriate non-dimensional fusion temperature of $\theta_f = 0.25$ results in $Nu = 5.1687$ ($Ra = 10^5$) and $Nu = 10.112$ ($Ra = 10^6$). Thus, a relative heat transfer enhancement of about 10% can be achieved compared to the base fluid for both the cases of $Ra = 10^5$ and $Ra = 10^6$. By using an inappropriate fusion temperature of $\theta_f = 0.05$, this enhancement would be reduced to only about 4%.

Table 3 shows the effect of various nondimensional parameters of *Ste*, θ_f, λ, ρ_p/ρ_f, *Nc* and *Nv* on the average Nusselt number in the cavity. The effect of these parameters on the average Nusselt number can be non-linear. However, here as a rough simulation of the behavior of these parameters, the effect of the variation of these parameters around their default values is studied. The increases of *Nc* and λ increase the average Nusselt number, and the increases in *Nv* and *Ste* decrease the average Nusselt number. The change of density ratio (ρ_p/ρ_f) does not show a noteworthy effect on the average Nusselt number. The increase in θ_f enhances the average Nusselt number. However, it should be noted that the effect of variation of θ_f was studied in Fig. 7(a) and a non-linear behavior was observed. The results of this table are in agreement with the graphical results of Fig. 7(a) for *Nu* as a function of θ_f, but the trend of the behavior of θ_f will be changed for θ_f higher than 0.5.

Comparing the Nusselt number results of this table with the Nusselt number of a pure fluid ($Nu = 4.7206$) shows that the presence of NEPCMs enhanced the heat transfer in the cavity for all of the cases.

5. Conclusion

The natural convection flow of a dilute suspension of a base fluid and NEPCM nanoparticles was addressed in this study. There was a free convection flow in the cavity, due to buoyancy effects. The NEPCM particles, as a part of the mixture, circulate in the cavity with the free convection flow. The contribution of the latent heat energy release and absorption of the NEPCM nanoparticles due to phase change was taken into account. The governing equations for the conservation of mass, momentum, and energy were introduced and transformed into a non-dimensional form. Then, the finite element method was employed to solve the governing equations associated with the boundary conditions. Grid checks and validations were performed to ensure the accuracy and correctness of the solutions. The main outcomes can be summarized as follows:

(1) The presence of NEPCMs contributes to heat transfer enhancement by improving the thermal conductivity and increasing the heat capacity of the suspension at the fusion temperature of the NEPCM particles. However, the presence of the NEPCM nanoparticles also has some drawbacks, such as an increase of dynamic viscosity, a decrease of sensible heat capacity, and a decrease of buoyancy forces, which lead to a decrease of heat transfer. The general trend of the results demonstrates a heat transfer enhancement by using NEPCM particles.

(2) The non-dimensional fusion temperature is a key parameter in enhancing the heat transfer in the cavity. When the fusion temperature of the PCM cores is close to the hot or cold wall temperatures, the heat transfer enhancement due to phase change is low. Deviation of the fusion temperature from the wall temperatures increases the effectiveness of the NEPCM particles in terms of heat transfer enhancement. The best heat transfer performance can be obtained with a non-dimensional fusion temperature in the range of $\theta_f = 0.25$-$\theta_f = 0.75$.

(3) An increase of the latent heat of the PCM cores (i.e., a decrease of *Ste*) increases the average Nusselt number in the cavity. Thus, using phase change materials with higher latent heat of phase change can further enhance heat transfer.

One of the advantages of using phase change materials is the control of the surface temperature and its uniformity with a specific fusion temperature. Hence, the study of natural convection in a cavity with boundaries subject to heat flux and analysis of the temperature uniformity of the wall surface can be the subjects of future studies.

Conflict of interest

The authors clarify that there is no conflict of interest for report.

Acknowledgments

This project is supported by 111 projects (B18002).

Appendix A. Supplementary material

Supplementary data to this article can be found online at https://doi.org/10.1016/j.ijheatmasstransfer.2019.04.037.

References

[1] W. Su, J. Darkwa, G. Kokogiannakis, Review of solid–liquid phase change materials and their encapsulation technologies, Renew. Sustain. Energy Rev. 48 (2015) 373–391, https://doi.org/10.1016/J.RSER.2015.04.044.
[2] G. Fang, H. Li, F. Yang, X. Liu, S. Wu, Preparation and characterization of nano-encapsulated n-tetradecane as phase change material for thermal energy storage, Chem. Eng. J. 153 (2009) 217–221, https://doi.org/10.1016/J.CEJ.2009.06.019.
[3] X. Qiu, W. Li, G. Song, X. Chu, G. Tang, Fabrication and characterization of microencapsulated n-octadecane with different crosslinked

methylmethacrylate-based polymer shells, Sol. Energy Mater. Sol. Cells 98 (2012) 283–293, https://doi.org/10.1016/J.SOLMAT.2011.11.018.
[4] A. Jamekhorshid, S.M. Sadrameli, M. Farid, A review of microencapsulation methods of phase change materials (PCMs) as a thermal energy storage (TES) medium, Renew. Sustain. Energy Rev. 31 (2014) 531–542, https://doi.org/10.1016/J.RSER.2013.12.033.
[5] K. Pielichowska, K. Pielichowski, Phase change materials for thermal energy storage, Prog. Mater Sci. 65 (2014) 67–123, https://doi.org/10.1016/J.PMATSCI.2014.03.005.
[6] A. Nematpour Keshteli, M. Sheikholeslami, Nanoparticle enhanced PCM applications for intensification of thermal performance in building: a review, J. Mol. Liq. 274 (2019) 516–533, https://doi.org/10.1016/J.MOLLIQ.2018.10.151.
[7] X. Huang, G. Alva, Y. Jia, G. Fang, Morphological characterization and applications of phase change materials in thermal energy storage: a review, Renew. Sustain. Energy Rev. 72 (2017) 128–145, https://doi.org/10.1016/J.RSER.2017.01.048.
[8] P. Moreno, C. Solé, A. Castell, L.F. Cabeza, The use of phase change materials in domestic heat pump and air-conditioning systems for short term storage: a review, Renew. Sustain. Energy Rev. 39 (2014) 1–13, https://doi.org/10.1016/J.RSER.2014.07.062.
[9] M. Sheikholeslami, Numerical modeling of nano enhanced PCM solidification in an enclosure with metallic fin, J. Mol. Liq. 259 (2018) 424–438, https://doi.org/10.1016/J.MOLLIQ.2018.03.006.
[10] N. Bondareva, M. Sheremet, Natural convection melting of nano-enhanced phase change material in a cavity with finned copper profile, MATEC Web Conf. 240 (2018) 01006, https://doi.org/10.1051/matecconf/201824001006.
[11] R. Hossain, S. Mahmud, A. Dutta, I. Pop, Energy storage system based on nanoparticle-enhanced phase change material inside porous medium, Int. J. Therm. Sci. 91 (2015) 49–58, https://doi.org/10.1016/J.IJTHERMALSCI.2014.12.023.
[12] M. Ghalambaz, A. Doostani, E. Izadpanahi, A.J. Chamkha, Phase-change heat transfer in a cavity heated from below: The effect of utilizing single or hybrid nanoparticles as additives, J. Taiwan Inst. Chem. Eng. 72 (2017), https://doi.org/10.1016/j.jtice.2017.01.010.
[13] S.R. Hosseini, M. Sheikholeslami, M. Ghasemian, D.D. Ganji, Nanofluid heat transfer analysis in a microchannel heat sink (MCHS) under the effect of magnetic field by means of KKL model, Powder Technol. 324 (2018) 36–47, https://doi.org/10.1016/J.POWTEC.2017.10.043.
[14] M. Sheikholeslami, M.K. Sadoughi, Simulation of CuO-water nanofluid heat transfer enhancement in presence of melting surface, Int. J. Heat Mass Transf. 116 (2018) 909–919, https://doi.org/10.1016/J.IJHEATMASSTRANSFER.2017.09.086.
[15] A.J. Chamkha, A. Doostanidezfuli, E. Izadpanahi, M. Ghalambaz, Phase-change heat transfer of single/hybrid nanoparticles-enhanced phase-change materials over a heated horizontal cylinder confined in a square cavity, Adv. Powder Technol. 28 (2017), https://doi.org/10.1016/j.apt.2016.10.009.
[16] R. Elbahjaoui, H. El Qarnia, Transient behavior analysis of the melting of nanoparticle-enhanced phase change material inside a rectangular latent heat storage unit, Appl. Therm. Eng. 112 (2017) 720–738, https://doi.org/10.1016/J.APPLTHERMALENG.2016.10.115.
[17] I. Hashim, A.I. Alsabery, M.A. Sheremet, A.J. Chamkha, Numerical investigation of natural convection of Al2O3-water nanofluid in a wavy cavity with conductive inner block using Buongiorno's two-phase model, Adv. Powder Technol. (2018), https://doi.org/10.1016/J.APT.2018.11.017.
[18] A.I. Alsabery, M.A. Sheremet, A.J. Chamkha, I. Hashim, Impact of nonhomogeneous nanofluid model on transient mixed convection in a double lid-driven wavy cavity involving solid circular cylinder, Int. J. Mech. Sci. 150 (2019) 637–655, https://doi.org/10.1016/J.IJMECSCI.2018.10.069.
[19] C. Sivaraj, M.A. Sheremet, MHD natural convection and entropy generation of ferrofluids in a cavity with a non-uniformly heated horizontal plate, Int. J. Mech. Sci. 149 (2018) 326–337, https://doi.org/10.1016/J.IJMECSCI.2018.10.017.
[20] M. Ghalambaz, M.A. Sheremet, S.A.M. Mehryan, F.M. Kashkooli, I. Pop, Local thermal non-equilibrium analysis of conjugate free convection within a porous enclosure occupied with Ag–MgO hybrid nanofluid, J. Therm. Anal. Calorim. (2018) 1–18, https://doi.org/10.1007/s10973-018-7472-8.
[21] A. Tahmasebi, M. Mahdavi, M. Ghalambaz, Local thermal nonequilibrium conjugate natural convection heat transfer of nanofluids in a cavity partially filled with porous media using Buongiorno's model, Numer. Heat Transf. Part A Appl. 73 (2018) 254–276, https://doi.org/10.1080/10407782.2017.1422632.
[22] A.I. Alsabery, T. Armaghani, A.J. Chamkha, M.A. Sadiq, I. Hashim, Effects of two-phase nanofluid model on convection in a double lid-driven cavity in the presence of a magnetic field, Int. J. Numer. Meth. Heat Fluid Flow (2018), https://doi.org/10.1108/HFF-07-2018-0386, HFF-07-2018-0386.
[23] A.I. Alsabery, T. Tayebi, A.J. Chamkha, I. Hashim, Effects of two-phase nanofluid model on natural convection in a square cavity in the presence of an adiabatic inner block and magnetic field, Int. J. Numer. Meth. Heat Fluid Flow 28 (2018) 1613–1647, https://doi.org/10.1108/HFF-10-2017-0425.
[24] H. Reza Seyf, M.R. Wilson, Y. Zhang, H.B. Ma, Flow and heat transfer of nanoencapsulated phase change material slurry past a unconfined square cylinder, J. Heat Transfer 136 (2014), https://doi.org/10.1115/1.4025903, 051902.
[25] H.R. Seyf, Z. Zhou, H.B. Ma, Y. Zhang, Three dimensional numerical study of heat-transfer enhancement by nano-encapsulated phase change material slurry in microtube heat sinks with tangential impingement, Int. J. Heat Mass Transf. 56 (2013) 561–573, https://doi.org/10.1016/J.IJHEATMASSTRANSFER.2012.08.052.
[26] C.-J. Ho, W.-C. Chen, W.-M. Yan, Experimental study on cooling performance of minichannel heat sink using water-based MEPCM particles, Int. Commun. Heat Mass Transf. 48 (2013) 67–72, https://doi.org/10.1016/J.ICHEATMASSTRANSFER.2013.08.023.
[27] C.J. Ho, J.B. Huang, P.S. Tsai, Y.M. Yang, Water-based suspensions of Al2O3 nanoparticles and MEPCM particles on convection effectiveness in a circular tube, Int. J. Therm. Sci. 50 (2011) 736–748, https://doi.org/10.1016/J.IJTHERMALSCI.2010.11.015.
[28] C.J. Ho, W.-C. Chen, W.-M. Yan, Correlations of heat transfer effectiveness in a minichannel heat sink with water-based suspensions of Al2O3 nanoparticles and/or MEPCM particles, Int. J. Heat Mass Transf. 69 (2014) 293–299, https://doi.org/10.1016/J.IJHEATMASSTRANSFER.2013.10.030.
[29] S. Kuravi, K.M. Kota, J. Du, L.C. Chow, Numerical investigation of flow and heat transfer performance of nano-encapsulated phase change material slurry in microchannels, J. Heat Transfer 131 (2009), https://doi.org/10.1115/1.3084123 062901.
[30] M. Mohib Ur Rehman, Z.G. Qu, R.P. Fu, Three-dimensional numerical study of laminar confined slot jet impingement cooling using slurry of nano-encapsulated phase change material, J. Therm. Sci. 25 (2016) 431–439, https://doi.org/10.1007/s11630-016-0881-8.
[31] L. Chai, R. Shaukat, L. Wang, H.S. Wang, A review on heat transfer and hydrodynamic characteristics of nano/microencapsulated phase change slurry (N/MPCS) in mini/microchannel heat sinks, Appl. Therm. Eng. 135 (2018) 334–349, https://doi.org/10.1016/J.APPLTHERMALENG.2018.02.068.
[32] X. Du, Y. Fang, X. Cheng, Z. Du, M. Zhou, H. Wang, Fabrication and characterization of flame-retardant nanoencapsulated n-octadecane with melamine-formaldehyde shell for thermal energy storage, ACS Sustain. Chem. Eng. 6 (2018) 15541–15549, https://doi.org/10.1021/acssuschemeng.8b03980.
[33] B. Chen, X. Wang, R. Zeng, Y. Zhang, X. Wang, J. Niu, Y. Li, H. Di, An experimental study of convective heat transfer with microencapsulated phase change material suspension: Laminar flow in a circular tube under constant heat flux, Exp. Therm Fluid Sci. 32 (2008) 1638–1646, https://doi.org/10.1016/J.EXPTHERMFLUSCI.2008.05.008.
[34] K. Khanafer, K. Vafai, A critical synthesis of thermophysical characteristics of nanofluids, Int. J. Heat Mass Transf. 54 (2011) 4410–4428, https://doi.org/10.1016/J.IJHEATMASSTRANSFER.2011.04.048.
[35] E.L. Alisetti, S.K. Roy, Forced convection heat transfer to phase change material slurries in circular ducts, J. Thermophys. Heat Transf. 14 (2000) 115–118, https://doi.org/10.2514/2.6499.
[36] J. Buongiorno, Convective transport in nanofluids, J. Heat Transfer 128 (2006) 240, https://doi.org/10.1115/1.2150834.
[37] J. Buongiorno, D.C. Venerus, N. Prabhat, T. McKrell, J. Townsend, R. Christianson, Y.V. Tolmachev, P. Keblinski, L. Hu, J.L. Alvarado, I.C. Bang, S.W. Bishnoi, M. Bonetti, F. Botz, A. Cecere, Y. Chang, G. Chen, H. Chen, S.J. Chung, M. K. Chyu, S.K. Das, R. Di Paola, Y. Ding, F. Dubois, G. Dzido, J. Eapen, W. Escher, D. Funfschilling, Q. Galand, J. Gao, P.E. Gharagozloo, K.E. Goodson, J.G. Gutierrez, H. Hong, M. Horton, K.S. Hwang, C.S. Iorio, S.P. Jang, A.B. Jarzebski, Y. Jiang, L. Jin, S. Kabelac, A. Kamath, M.A. Kedzierski, L.G. Kieng, C. Kim, J.-H. Kim, S. Kim, S.H. Lee, K.C. Leong, I. Manna, B. Michel, R. Ni, H.E. Patel, J. Philip, D. Poulikakos, C. Reynaud, R. Savino, P.K. Singh, P. Song, T. Sundararajan, E. Timofeeva, T. Tritcak, A.N. Turanov, S. Van Vaerenbergh, D. Wen, S. Witharana, C. Yang, W.-H. Yeh, X.-Z. Zhao, S.-Q. Zhou, A benchmark study on the thermal conductivity of nanofluids, J. Appl. Phys. 106 (2009), https://doi.org/10.1063/1.3245330 094312.
[38] M.A. Kedzierski, D. Venerus, J. Buongiorno, R. Christianson, J. Townsend, I.C. Bang, G. Chen, S.J. Chung, M. Chyu, H. Chen, Y. Ding, F. Dubois, G. Dzido, D. Funfschilling, Q. Galand, J. Gao, H. Hong, M. Horton, L. Hu, C. Iorio, A. Jarzebski, Y. Jiang, S. Kabelac, C. Kim, J.H. Kim, S. Kim, T. McKrell, R. Ni, J. Philip, N. Prabhat, P. Song, S. Van Vaerenbergh, D. Wen, S. Witharana, X.-Z. Zhao, S.-Q. Zhou, Viscosity measurements on colloidal dispersions (nanofluids) for heat transfer applications | NIST, Appl. Rheol. J. (2010) (accessed 15.11.18).
[39] A. Zaraki, M. Ghalambaz, A.J. Chamkha, M. Ghalambaz, D. De Rossi, Theoretical analysis of natural convection boundary layer heat and mass transfer of nanofluids: Effects of size, shape and type of nanoparticles, type of base fluid and working temperature, Adv. Powder Technol. 26 (2015), https://doi.org/10.1016/j.apt.2015.03.012.
[40] O.C. Zienkiewicz, R.L. Robert, L. Taylor, The Finite Element Method for Solid and Structural Mechanics, Elsevier Butterworth-Heinemann, 2005 (accessed 24.11.18).
[41] O. Turan, A. Sachdeva, N. Chakraborty, R.J. Poole, Laminar natural convection of power-law fluids in a square enclosure with differentially heated side walls subjected to constant temperatures, J. Nonnewton. Fluid Mech. 166 (2011) 1049–1063, https://doi.org/10.1016/J.JNNFM.2011.06.003.
[42] K. Kahveci, Buoyancy driven heat transfer of nanofluids in a tilted enclosure, J. Heat Transfer 132 (2010), https://doi.org/10.1115/1.4000744 062501.
[43] Q.-H. Deng, G.-F. Tang, Numerical visualization of mass and heat transport for conjugate natural convection/heat conduction by streamline and heatline, Int. J. Heat Mass Transf. 45 (2002) 2373–2385, https://doi.org/10.1016/S0017-9310(01)00316-7.
[44] R. Anandalakshmi, T. Basak, Heat flow visualization for natural convection in rhombic enclosures due to isothermal and non-isothermal heating at the bottom wall, Int. J. Heat Mass Transf. 55 (2012) 1325–1342, https://doi.org/10.1016/J.IJHEATMASSTRANSFER.2011.09.006.

[45] Y. Khakpour, J. Seyed-Yagoobi, Natural convection in an enclosure with micro encapsulated phase change material: experimental and numerical study, in: 11th AIAA/ASME Jt. Thermophys. Heat Transf. Conf., American Institute of Aeronautics and Astronautics, Reston, Virginia, 2014. https://doi.org/10.2514/6.2014-2553.

[46] Y. Rao, F. Dammel, P. Stephan, G. Lin, Convective heat transfer characteristics of microencapsulated phase change material suspensions in minichannels, Heat Mass Transf. 44 (2007) 175–186, https://doi.org/10.1007/s00231-007-0232-0.

[47] W.Q. Li, H. Wan, T.T. Jing, Y.B. Li, P.J. Liu, G.Q. He, F. Qin, Microencapsulated phase change material (MEPCM) saturated in metal foam as an efficient hybrid PCM for passive thermal management: A numerical and experimental study, Appl. Therm. Eng. 146 (2019) 413–421, https://doi.org/10.1016/J.APPLTHERMALENG.2018.10.006.

[48] Y.-H. Siao, W.-M. Yan, C.-M. Lai, Transient characteristics of thermal energy storage in an enclosure packed with MEPCM particles, Appl. Therm. Eng. 88 (2015) 47–53, https://doi.org/10.1016/J.APPLTHERMALENG.2014.11.059.

[49] M. Ghalambaz, H. Jin, D. Wen, I. Pop, Boundary layer natural convection flow heat and mass transfer of nano-encapsulated phase change materials (NEPCMs) over a flat plate, Int. Commun. Heat Mass Transf. (n.d.) (submitted for publications).